



UNIVERSITY
OF WOLLONGONG
AUSTRALIA

University of Wollongong
Research Online

Australian Institute for Innovative Materials - Papers

Australian Institute for Innovative Materials

2018

Synergistic amplification of catalytic hydrogen generation by a thin-film conducting polymer composite

Mohammed Alsultan

University of Wollongong, University of Mosul, mfka287@uowmail.edu.au

Jaecheol Choi

University of Mosul, jc878@uowmail.edu.au

Rouhollah Jalili

University of Mosul, rjalili@uow.edu.au

Pawel W. Wagner

University of Mosul, pawel@uow.edu.au

Gerhard F. Swiegers

University of Mosul, swiegers@uow.edu.au

Publication Details

Alsultan, M., Choi, J., Jalili, R., Wagner, P. & Swiegers, G. F. (2018). Synergistic amplification of catalytic hydrogen generation by a thin-film conducting polymer composite. *Catalysis Science & Technology*, 8 (16), 4169-4179.

Research Online is the open access institutional repository for the University of Wollongong. For further information contact the UOW Library:
research-pubs@uow.edu.au

Synergistic amplification of catalytic hydrogen generation by a thin-film conducting polymer composite

Abstract

This work reports a composite of poly[3,4-ethylenedioxythiophene] (PEDOT) that is notably more catalytically active for hydrogen generation than the industry-standard benchmark catalyst, Pt, under the same conditions. A PEDOT thin-film containing nanoparticulate Ni (nano-Ni) and reduced graphene oxide (rGO) in the specific molar ratio of 5.6 (C; PEDOT) : 1 (Ni) : 5.2 (C; other), (photo)catalytically generated H₂ at 3.6 mA cm⁻² (including ca. 0.2 mA cm⁻² due to the light illumination) after 3 h at -0.75 V (vs. Ag/AgCl) in 0.05 M H₂SO₄/0.2 M Na₂SO₄ under 0.25 sun. A control nano-Ni/rGO film containing the same quantities of nano-Ni and rGO but without any PEDOT, yielded 2.1 mA cm⁻², indicating that the PEDOT synergistically amplified the above result by 71%. Other ratios of the above PEDOT composite produced notably lower activities. Control PEDOT, PEDOT/nano-Ni, and PEDOT/rGO films were an order of magnitude less catalytically active. A control bare Pt electrode produced only 2.2 mA cm⁻² under the same conditions. Studies suggested the origin of the synergistic amplification to involve the PEDOT electrically connecting the largest number of active sites by the shortest, most efficient pathways for hole transport. These results confirm the proposition that thin-film conducting polymers involving very specific, optimum ratios of catalyst density to thickness may synergistically amplify catalysis.

Disciplines

Engineering | Physical Sciences and Mathematics

Publication Details

Alsultan, M., Choi, J., Jalili, R., Wagner, P. & Swiegers, G. F. (2018). Synergistic amplification of catalytic hydrogen generation by a thin-film conducting polymer composite. *Catalysis Science & Technology*, 8 (16), 4169-4179.



Synergistic Amplification of Catalytic Hydrogen Generation by a Thin-Film Conducting Polymer Composite

Mohammed Alsultan,^{a,b} Jaecheol Choi,^a Rouhollah Jalili,^a Pawel Wagner^a and Gerhard F. Swiegers*^a

Received 00th January 20xx,
Accepted 00th January 20xx

DOI: 10.1039/x0xx00000x

www.rsc.org/

This work reports a composite of poly(3,4-ethylenedioxythiophene) (PEDOT) that is notably more catalytically active for hydrogen generation than the industry-standard benchmark catalyst, Pt, under the same conditions. A PEDOT thin-film containing nanoparticulate Ni (nano-Ni) and reduced graphene oxide (rGO) in the specific molar ratio of 5.6 (C; PEDOT) : 1 (Ni) : 5.2 (C; other), (photo)catalytically generated H₂ at 3.6 mA/cm² (including ca. 0.2 mA/cm² due to the light illumination) after 3 h at -0.75 V (vs Ag/AgCl) in 0.05 M H₂SO₄/0.2 M Na₂SO₄ under 0.25 sun. A control nano-Ni/rGO film containing the same quantities of nano-Ni and rGO but without any PEDOT, yielded 2.1 mA/cm², indicating that the PEDOT synergistically amplified the above result by 71%. Other ratios of the above PEDOT composite produced notably lower activities. Control PEDOT, PEDOT/nano-Ni, and PEDOT/rGO films were an order of magnitude less catalytically active. A control bare Pt electrode produced only 2.2 mA/cm² under the same conditions. Studies suggested the origin of the synergistic amplification to involve the PEDOT electrically connecting the largest number of active sites by the shortest, most efficient pathways for hole transport. These results confirm the proposition that thin-film conducting polymers involving very specific, optimum ratios of catalyst density to thickness may synergistically amplify catalysis.

Introduction

Hydrogen (H₂) is widely considered to be the ideal fuel for a future clean, sustainable, and environmentally-friendly energy technology.^{1,2} Not only does hydrogen have a high energy density (122 kJ/g) compared to fossil fuels (e.g. gasoline, 40 kJ/g),^{3,4} but it is also non-polluting, generating only water as a waste product. For these reasons, the production of hydrogen via water-splitting in electrochemical (EC) or photo-electrochemical (PEC) cells, has been of particular interest. Conducting polymers (CPs) exhibit potentially useful properties as porous, conductive, and light-harvesting supports in catalytic hydrogen-generating ECs/PECs.⁵ Of the various, available CPs, poly(3,4-ethylenedioxythiophene) (PEDOT) is widely considered to be the most practical, thanks to its stability, capacity for electrochemical switching, conductivity, processability, and, in the case of photocatalysis, also its transparency to visible light.⁶ As a catalyst of the hydrogen evolution reaction (HER) (2H⁺+2e⁻→H₂) however, virgin PEDOT generates only very small current densities that typically fall in the low μA/cm² range. For this reason, PEDOT is only of practical interest in combination with other materials and conductors, such as non-conducting polymers (e.g. polyethyleneglycol, PEG),⁷ carbon materials (e.g. single wall

carbon nanotubes),⁸ metallic nanoparticles (e.g. Pd),⁹ and light-activated semiconductors (e.g. Si).¹⁰ While a number of studies have examined such thin-film PEDOT composites as HER catalysts, few have considered how PEDOT could be deployed to promote the highest possible catalytic activity. One study that did consider this question involved a PEDOT-PEG composite that was deposited on a Au-coated Gortex substrate.^{7(b)} That system yielded sustained current densities for HER catalysis of 2.2 mA/cm² at -0.35 V (vs SCE) in strong acid (1 M H₂SO₄), that were closely comparable to that produced by the industry benchmark HER catalyst, Pt, under the same conditions. The high activity of the PEDOT-PEG derived from the large surface area of the Gortex substrate. The PEG also increased proton diffusion and overall conductivity.^{7(b)} To the best of our knowledge, this system is the most active reported PEDOT-based HER electrocatalyst as a proportion of the benchmark catalytic activity of Pt under the same settings.

In recent work we investigated the conditions under which thin-film conducting polymer supports like PEDOT may be induced to synergistically amplify water oxidation catalysis beyond what may be expected from the catalyst alone.¹¹ That work suggested that the conducting polymer should electrically connect the largest number of catalytic sites by the shortest, least-resistive pathways to thereby achieve: (1) the greatest active area that is also: (2) the most responsive to the applied bias (minimizing the Tafel slope).¹¹ That is, the connectivity, electron conductivity and catalytic capacity of the film should be matched. This was proposed to occur at very specific, optimum ratios of catalyst density to film conductivity and thickness.

^a Department of Science, University of Mosul, Mosul, Iraq

^b Intelligent Polymer Research Institute and ARC Centre of Excellence for Electromaterials Science, University of Wollongong, Wollongong, NSW 2522, Australia. Email: Swiegers@uow.edu.au

Electronic Supplementary Information (ESI) available: Photographs and diagrams of cell used for gas studies; Pourbaix diagram for Ni, GC trace of the gas collected. See DOI: 10.1039/x0xx00000x

In this work we have sought to examine the same question as it relates to hydrogen generation catalysis, using a composite thin film comprising of PEDOT, nanoparticulate Ni (nano-Ni) as a catalyst, and reduced graphene oxide (rGO) as a conductor. Nano-Ni is an H₂-generating catalyst, while graphene oxide, which is normally insulating and hydrophobic,^{12,13} becomes conducting¹⁴⁻¹⁶ when reduced to rGO.¹⁷⁻²⁴ A key difference with the earlier work¹¹ is that the PEDOT conducting polymer is in its non-conducting form under the cathodic voltage bias conditions needed for hydrogen generation catalysis. As such, it was not clear whether synergistic amplifications beyond what may be expected from the catalyst alone could be achieved at all, nor whether they would follow the general principles that were observed for water oxidation catalysis.

We report that a 0.61 μm thick film (4.2 cm²) of PEDOT containing the very specific ratio of 125 mg nano-Ni and 5.4 mg rGO yields a sustained current density of 3.6 mA/cm² (including ca. 0.2 mA/cm² due to the light illumination) at -0.75 V (vs Ag/AgCl) in 0.05 M H₂SO₄/0.2 M Na₂SO₄ after 3 h under 0.25 sun. Other ratios produced notably lower activities. This was 64% higher than a benchmark, control bare Pt electrode, which produced 2.2 mA/cm² under identical conditions. It was also higher than a control film that contained only 125 mg nano-Ni and 5.6 mg rGO, without any PEDOT. The above settings represent the most favorable conditions for HER catalysis under which the nano-Ni is not susceptible to dissolution. Studies show that, like the earlier study involving water oxidation catalysis, the synergistic amplification appears to have derived from the PEDOT connecting the largest number of catalytic sites by the shortest, most efficient pathway for charge carrier conduction. In this case however, the charge carriers were holes (h⁺) and the conduction process involved hole transport. The above thin-film appears to be the most active PEDOT-based HER catalyst yet reported as a proportion of the catalytic activity of Pt under the same conditions.

Results and Discussion

CV studies of control films of nano-Ni/rGO on FTO glass

In the first stage of this study, we sought to determine the most favourable pH and voltage bias conditions under which HER catalysis by the proposed composite PEDOT/nano-Ni/rGO thin films could be studied without degradation of the films. As PEDOT is known to be stable under even strongly reducing conditions in 1 M H₂SO₄ (pH 0.3),^{7(b)} we studied thin-film mixtures of nano-Ni and rGO only (without any PEDOT) that had been spin-coated onto FTO glass and dried. These films proved to bind robustly to the FTO glass. The nano-Ni had an average diameter of 20 nm; the rGO was prepared as described in the Experimental Section.

To assess the best conditions for HER catalysis by these thin-films, without degradation, we measured their CVs under reducing conditions (-0.25 V to -1.1 V vs Ag/AgCl) without light illumination, over a range of pHs (0-12). At a pH of 0, the nano-Ni/rGO films delaminated from the FTO glass, suggesting that one of the components degraded. However, the films were stable to delamination at pH's of 1 and above.

Films having a wide variety of weight ratios of nano-Ni : rGO were studied. All displayed characteristic HER catalytic currents (Figure 1). One film, having the weight ratio of 125 mg nano-Ni : 6

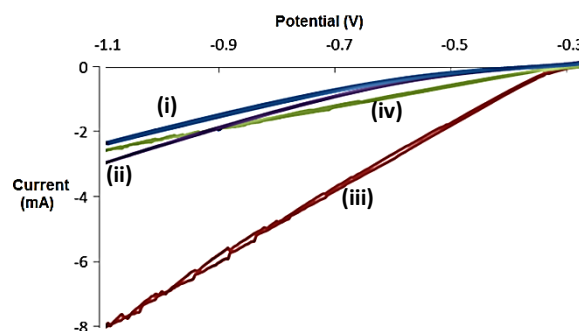


Figure 1. Cyclic voltammograms (vs Ag/AgCl) in 0.05 M H₂SO₄/0.2 M Na₂SO₄, without light illumination, of FTO glass slides having 1 cm² active geometric area, coated with: (i)-(ii) nano-Ni/rGO (ratio 125 mg nano-Ni : 6 mg rGO), (i) immediately after preparation and (ii) after 15 scans; or: (iii)-(iv) 100 nm of sputter-coated Pt, (iii) immediately after preparation and (iv) after 15 scans. Scan rate: 5 mV/s.

mg rGO appeared to be the most active. The relative current densities of this film at -1.1 V (vs Ag/AgCl) during scanning increased from ca. 1.2 mA/cm² at pH 12 to ca. 3 mA/cm² at pH 1. By contrast, an equivalent, sputtered, bare Pt film on an FTO glass slide yielded, at pH 1, an onset potential of 0.32 V and a current density of ca. 8 mA/cm² at -1.1 V (vs Ag/AgCl) (Figure 1).

It therefore appeared advantageous to study the proposed PEDOT/Nano-Ni/rGO composite films at a pH of 1. However, the Pourbaix diagram for Ni (Figure S2) indicated that at pH 1, Ni is susceptible to dissolution with subsequent formation of soluble Ni(II) at potentials more positive than -0.375 V vs SHE (-0.605 V vs Ag/AgCl). At potentials more negative than this, Ni is favored to remain a solid metal. Accordingly, it was decided to study the proposed PEDOT/nano-Ni/rGO composite films on FTO glass slides in 0.05 M H₂SO₄ / 0.2 M Na₂SO₄ (pH 1) at potentials of -0.75 V vs Ag/AgCl, which was well clear of the -0.605 V threshold.

Chronoamperometric Studies of films of Nano-Ni, rGO, PEDOT, PEDOT/Nano-Ni, PEDOT/rGO, and PEDOT/Nano-Ni/rGO on FTO

In the second stage of this work, we prepared PEDOT thin-films incorporating nano-Ni and/or rGO on FTO glass, using vapour phase polymerization. This technique involved spin-coating a fixed, small volume of an ethanol solution of Fe(III)-pTS oxidant (100 mg) that may contain nano-Ni and/or rGO onto an FTO glass slide (4.2 cm²). The slide was then dried and suspended in a sealed flask above liquid 3,4-ethylenedioxythiophene (EDOT), causing the formation of a PEDOT film of 55-65 μm thickness. The film was thoroughly washed to remove excess Fe and then dried.

The following samples were prepared on FTO glass slides: (i) PEDOT alone (control), (ii) PEDOT containing nano-Ni alone (control), (iii) PEDOT containing rGO alone (control), and (iv) PEDOT containing various mixtures of nano-Ni and rGO. Each of the films were prepared by incorporating nano-Ni (0-250 mg) and/or rGO (0-6 mg) in the spin-coating solution for vapour-phase polymerisation, with a uniformly thin PEDOT layer then being formed around them.

Chronoamperograms were thereafter measured at -0.75 V vs Ag/AgCl for each sample, as a working electrode in 0.05 M H₂SO₄ / 0.2 M Na₂SO₄, with and without light illumination using a SolLux daylight MR16 halogen light bulb (0.25 sun intensity). The earlier prepared films of nano-Ni/rGO were also tested. A large Pt mesh

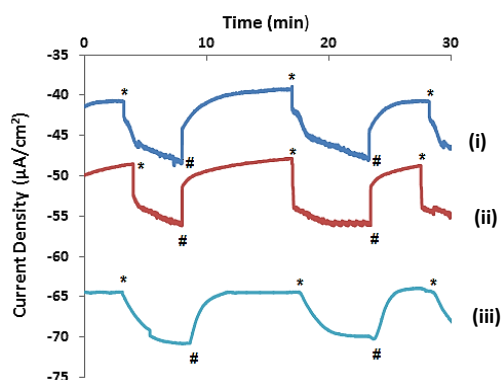


Figure 2. Chronoamperograms at -0.75 V (vs Ag/AgCl) in 0.05 M $\text{H}_2\text{SO}_4/0.2$ M Na_2SO_4 , after 3 h of operation, with and without light illumination (0.25 sun), of FTO glass slides coated with: (i) PEDOT alone, (ii) PEDOT/nano-Ni (125 mg nano-Ni), and (iii) PEDOT/rGO (5.4 mg rGO) (*='light on', #='light off'). Note that the data in graph (b) is in mA/cm^2 and therefore substantially larger than the data in graph (a), which is in $\mu\text{A}/\text{cm}^2$.

served as the counter electrode.

The control films containing PEDOT only produced low current densities of ca. $46 \mu\text{A}/\text{cm}^2$ (including a ca. $5 \mu\text{A}/\text{cm}^2$ photocurrent due to the light illumination) (Figure 2(a)(i)). A control PEDOT/nano-Ni film containing 125 mg nano-Ni yielded a higher, but still low current density of ca. $56 \mu\text{A}/\text{cm}^2$ (including ca. $9 \mu\text{A}/\text{cm}^2$ due to the light illumination) (Figure 2(a)(ii)). A control PEDOT/rGO film containing 5.4 mg rGO generated ca. $70 \mu\text{A}/\text{cm}^2$ (including ca. $6 \mu\text{A}/\text{cm}^2$ due to the light illumination) (Figure 2(a)(iii)). The low currents suggested that the PEDOT in the control films was coating the additives, particularly the nano-Ni catalyst, and blocking their catalytic activity.

Remarkably however, this did not prove to be a problem with the PEDOT/nano-Ni/rGO films, the most active of which contained 125 mg nano-Ni and 5.4 mg rGO, and yielded a current density of around $3.6 \text{ mA}/\text{cm}^2$ ($=3600 \mu\text{A}/\text{cm}^2$; including ca. $200 \mu\text{A}/\text{cm}^2$ due to the light illumination) (Figure 3(i)). This was about 60-times the current densities of the equivalent PEDOT-containing control films.

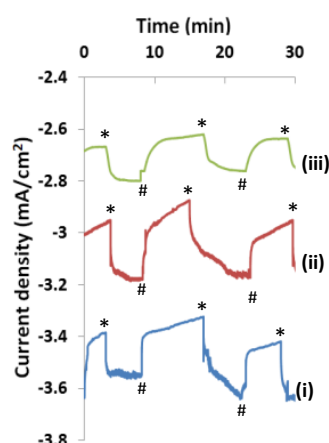


Figure 3. Chronoamperograms at -0.75 V (vs Ag/AgCl) in 0.05 M $\text{H}_2\text{SO}_4/0.2$ M Na_2SO_4 of FTO glass slides coated with: PEDOT/nano-Ni/rGO coatings after 3 h, with and without light illumination, where the coatings all contained 125 mg nano-Ni but with (b)(i) 5.4 mg rGO, (b)(ii) 6.0 mg rGO, or (b)(iii) 4.8 mg rGO (*='light on', #='light off').

An interesting feature of the performance of the PEDOT/nano-Ni/rGO films was what can only be described as an extreme sensitivity to the proportion of rGO present. The maximum catalytic performance was obtained when the film was made using 5.4 mg rGO in the spin-coated polymerisation solution (Figure 3(i)). The presence of a mere 0.6 mg more rGO (6.0 mg) or 0.6 mg less rGO (4.8 mg) in the film led to significant declines in the catalytic activity; namely, to $3.2 \text{ mA}/\text{cm}^2$ (Figure 3(ii)) and $2.8 \text{ mA}/\text{cm}^2$ (Figure 3(iii)), respectively, after 3 h under light illumination. Such extreme sensitivity is highly characteristic of a synergistic effect. A lesser sensitivity was seen for the nano-Ni, with the use of 135 mg or 110 mg decreasing the current by around 0.2 - $0.3 \text{ mA}/\text{cm}^2$. This is consistent with decreased light absorption.

The relatively slow rise times of the photocurrents after the light illumination was switched on has been observed before, and is characteristic of PEDOT.²⁵

As shown in Figure 4, the current density after 3 h under light illumination of the PEDOT/nano-Ni/rGO film containing 125 mg nano-Ni and 5.4 mg rGO ($3.6 \text{ mA}/\text{cm}^2$; Figure 4(i)) substantially exceeded that produced by an equivalent nano-Ni/rGO film, without PEDOT, containing the same ratio of nano-Ni : rGO of 125 mg : 5.4 mg ($2.1 \text{ mA}/\text{cm}^2$; Figure 4(ii)). The presence of the PEDOT therefore added at least $1.5 \text{ mA}/\text{cm}^2$ (or 70%) to the current density. Gas bubbles could be clearly seen to form and release on both films.

By contrast, the bare Pt control electrode generated only ca. $2.2 \text{ mA}/\text{cm}^2$ under the same conditions (Figure 4(iii)), which was comparable to the control nano-Ni/rGO film without PEDOT (Figure 4(ii)). Pt is well-known to initially be highly active in strong acids, with its activity thereafter declining sharply, especially over the first 1 h of operation.²⁶ As can be seen in Figure 4(iii), its current density stabilized at a level well below that of the PEDOT/nano-Ni/rGO thin-film composite (Figure 4(i)). The presence of the PEDOT was clearly critical to the superior performance.

Gas Collection Studies of PEDOT/Nano-Ni/rGO on FTO

To determine the identity of the bubbles formed on the most active

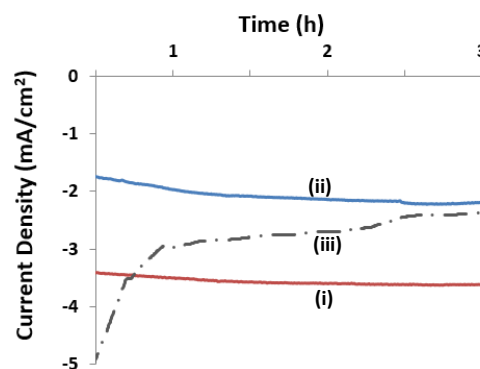


Figure 4. Chronoamperograms at -0.75 V (vs Ag/AgCl) in 0.05 M $\text{H}_2\text{SO}_4/0.2$ M Na_2SO_4 of FTO glass slides coated with: (i) PEDOT/nano-Ni/rGO (125 mg nano-Ni/5.4 mg rGO; with light illumination), (ii) nano-Ni/rGO without PEDOT (control) (125 mg nano-Ni/5.4 mg rGO; with light illumination), and (iii) bare Pt (control) (without light illumination).

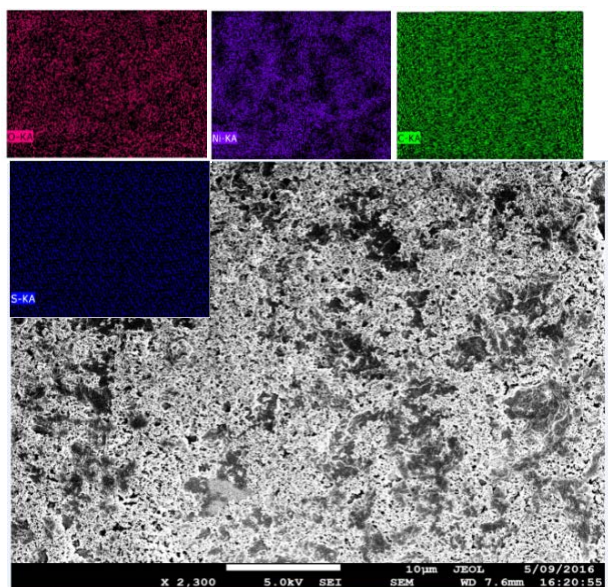


Figure 5. (a) Scanning electron microscope image of PEDOT/Nano-Ni/rGO containing 125 mg nano-Ni and 5.4 mg rGO. The inset images show the elemental distributions, using EDX, of: (b) O, (c) Ni, (d) C, (e) S, and (f) O, Ni, C, S together.

PEDOT/Nano-Ni/rGO thin film, we collected and tested the gas produced using a specialized, sealed cell (Figure S1) connected to a dedicated gas chromatograph (as described in the Experimental Section). In addition to the Ar carrier gas, the GC trace contained only a single peak whose retention time corresponded to hydrogen (Figure S3). Peaks due to other gases, including air nitrogen and/or oxygen, were notably absent. Gas bubbles formed on the Pt mesh counter electrode were separately shown to be pure oxygen using the same equipment.

The PEDOT/nano-Ni/rGO film therefore clearly catalysed the HER, with the nano-Ni/rGO components likely producing about 60% of the electrocatalytic effect and a synergistic amplification arising from the PEDOT accounting for the rest. The light-induced current density comprised only about 5% of the total.

Characterisation of the PEDOT/Nano-Ni/rGO Electrode

To determine the composition of the most active PEDOT/Nano-Ni/rGO film on the working electrode, elemental analysis studies were undertaken. Given that the quantity of material in such films was far below the minimum needed for an elemental analysis, multiple identical films were prepared, dried, carefully scraped off the FTO glass, and combined.

Analysis of the combined films indicated that they contained 22.00% Ni, 11.30% S, 48.70% C and no Fe. As only the PEDOT contained the element S, while rGO contained only C and the nano-Ni only Ni, it was possible to calculate the molar ratio of PEDOT : Ni : rGO to be 5.6 (C; PEDOT) : 1 (Ni) : 5.2 (C; other). As there are 6 C atoms in each PEDOT monomer, this equated to a ratio of 0.93 PEDOT monomers to every 1 Ni atom.

Scanning Electron Microscopy (SEM), Transmission Electron Microscopy (TEM), X-ray powder diffraction (XRD), and X-ray photoelectron spectroscopy (XPS) analyses were also performed on

the PEDOT/nano-Ni/rGO films prior to and after catalytic testing in order to assess structural and chemical changes in the catalytic film.

Figure 5(a) depicts a representative SEM image of the PEDOT/nano-Ni/rGO film after 3 h of operation, showing that its surface had developed a large number of vacant, nanoscopic pores. Indeed, the surface (and presumably the film) had become highly porous. This stands in contrast with Figure S4, which depicts the surface of the film prior to catalysis; no such pore structure was visible.

Measurements also showed that the above PEDOT/nano-Ni/rGO film, which had been prepared as a layer that was $0.61 \pm 2 \mu\text{m}$ thick, had swelled to $\sim 0.85 \mu\text{m}$ thickness upon immersion for 5 min in the 0.05 M H_2SO_4 / 0.2 M Na_2SO_4 electrolyte. After 3 h of operation, it was $\sim 0.98 \mu\text{m}$ thick. Clearly, the PEDOT/nano-Ni/rGO film swelled and became notably more porous during operation.

TEM showed the PEDOT to separately envelope each of the nano-Ni and the rGO platelets, with little contact between the nano-Ni and the rGO present. The PEDOT generally made seamless contact with the Ni lattice and with the rGO. There was no observable change to these interfaces, as seen using TEM, after 3 h of operation. This suggested that the porosity derived from the PEDOT itself becoming more porous and not from a change in the distribution or location of the nano-Ni and rGO within the PEDOT.

Figure 6 depicts X-ray powder diffraction (XRD) data for the PEDOT/nano-Ni/rGO film, as compared to control PEDOT (undoped), rGO, and its parent GO. The data did not substantially change over 3 h of operation. As can be seen, the XRD of the GO displayed a distinctive diffraction peak at $2\theta = 10.27^\circ$ due to the (002) carbon crystalline plane, revealing the presence of oxygen functional groups on the graphite sheets.²⁷⁻³² The XRD scan of the rGO shows, however, that the sharp peak at 10.2° had disappeared and been replaced by a new broad peak centred at 22.90° , consistent with the oxygen

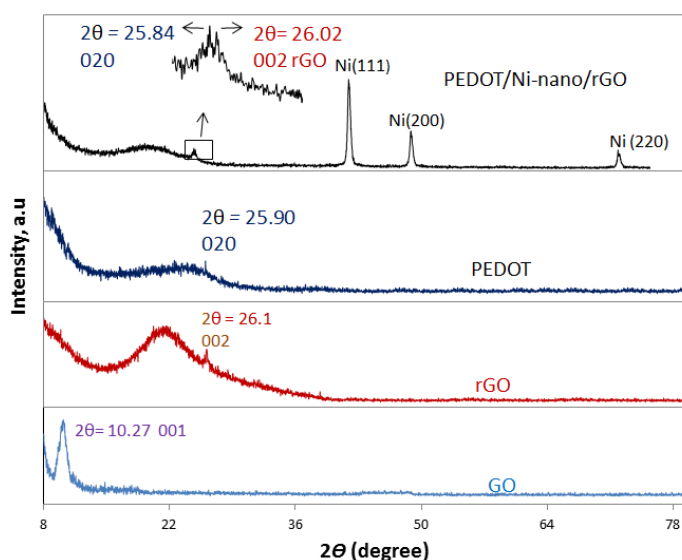


Figure 6. Powder X-ray diffraction (XRD) of PEDOT/Nano-Ni/rGO containing 125 mg nano-Ni and 5.4 mg rGO, relative to control PEDOT, control rGO, and control GO.

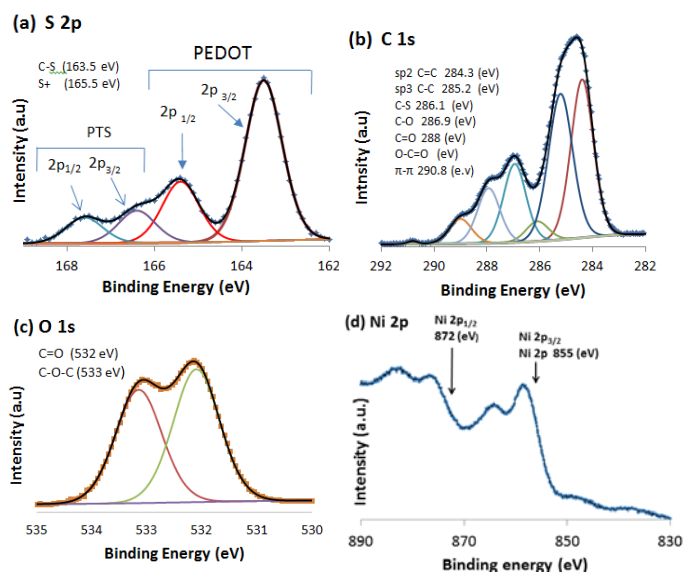


Figure 7. X-ray photoelectron spectroscopy (XPS) of PEDOT/Nano-Ni/rGO containing 125 mg nano-Ni and 5.4 mg rGO, showing measured data (individual data points) and modelled data (solid black lines) for the: (a) S 2p, (b) C 1s, (c) O 1s, (d) Ni 2p spectra.

functionalities being significantly reduced.^{33,34} As well, a clear diffraction peak at 26.1° , due to the (002) plane in the short-range order of stacked graphene sheets, was visible.^{35,36} The XRD of pure PEDOT exhibited a peak at $2\theta = 25.90^\circ$ which could be attributed to the (020) reflection due to the intermolecular spacing of the polymer backbone.^{37,38} The XRD of the PEDOT/nano-Ni/rGO film also displayed a broad peak at $2\theta = 17-25^\circ$ due to the rGO, as well as two peaks at $2\theta = 25.84^\circ$ and 26.02° due to the combination of the PEDOT and the rGO. A pattern of three peaks at 44.52° , 51.80° and 76.35° were due to the Ni(111), Ni(200) and Ni(220) planes, confirming the presence of the face centered cubic (fcc) structure of nickel in the nanoparticles.³⁹

To determine whether the catalysis altered the chemical states and elemental composition of the PEDOT/nano-Ni/rGO film, it was analysed using XPS at the commencement of, and after 3 h of operation. The resulting spectra, which were substantially similar, are depicted by the individual data points in Figure 7. The modelled spectra, shown by the solid black lines in Figure 7, closely matched the experimental data, shown by the colour data points. The XPS spectra of the PEDOT/nano-Ni/rGO film did not substantially change if the rGO present was varied from 4.8 mg to 6.0 mg.

The main peaks corresponded to O 1s, C 1s, Ni 2p and S 2p. The O 1s and C 1s spectra were associated with both PEDOT and rGO, while the S 2s spectrum derived only from the PEDOT. The C 1s spectrum contained four deconvolution peaks at 284.5, 285.2, 286.90 and 289 eV (Figure 7(b)). The peak at 284.5 eV represented a sp^2 carbon hybrid, which related to the C=C binding energy. The peak at 285.2 eV represented a sp^3 carbon hybrid and related to C-S, C-C, and/or C-H binding energies. Finally, the peaks at 288.0 and 289.0 eV related to C=O and O-C=O binding energies, respectively.⁴⁰⁻⁴⁹ The S 2p

spectrum contained peaks at 163.5 and 165.5 eV, which related to the binding energy of the $2p_{3/2}$ and $2p_{1/2}$ that correspond to the C-S bond and S^+ . These were assigned to the S atoms of the PEDOT fragments. The other two small peaks relate to the $2p_{3/2}$ and $2p_{1/2}$ of the sulfonic groups in the PTS structure.⁵⁰⁻⁵³ The O 1s spectrum of the film displayed two peaks at 532 and 533.4 eV. These related to the binding energy of C=O and/or C-O bonds respectively.⁵⁴⁻⁵⁶ Finally, the Ni 2p spectra exhibited two main peaks at 855 and 872 eV, relating to 1/2 and 3/2 spin respectively.

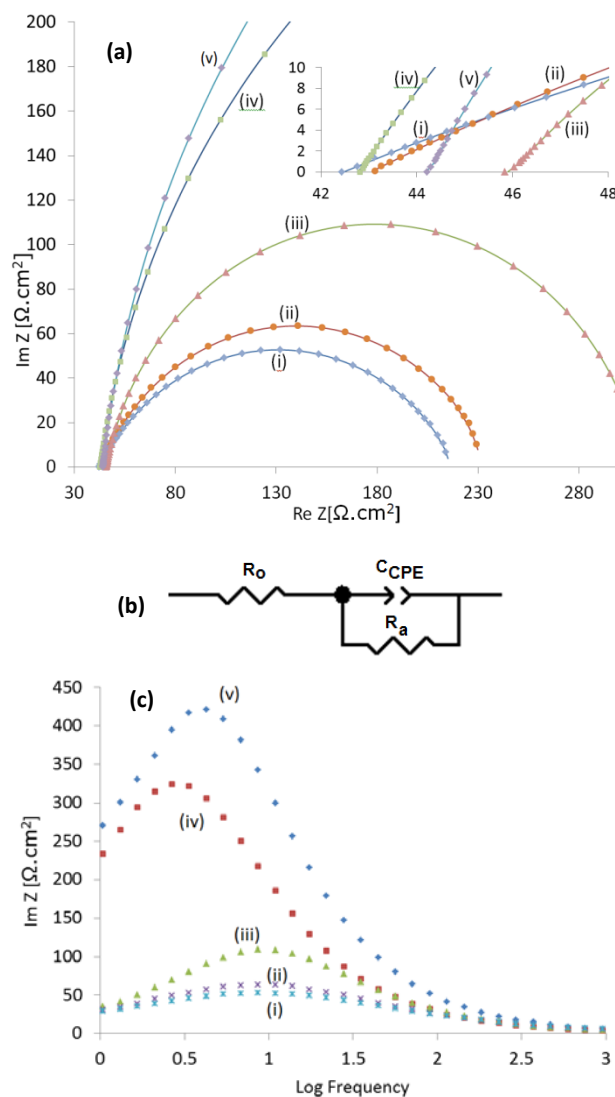


Figure 8. (a) Nyquist plot, (b) equivalent circuit, and (c) Bode plot; at -0.75 V (vs Ag/AgCl); showing measured data (individual data points) and modelled data (solid lines) (modelled using the equivalent circuit depicted in (b)), for: (i) PEDOT/nano-Ni/rGO containing 125 mg nano-Ni and 5.4 mg rGO (with light illumination), (ii) PEDOT/nano-Ni/rGO containing 125 mg nano-Ni and 5.4 mg rGO (without light illumination), (iii) control nano-Ni/rGO (without PEDOT) containing 125 mg nano-Ni and 5.4 mg rGO (with light illumination), (iv) control PEDOT only (with light illumination), and (v) control PEDOT only (without light illumination).

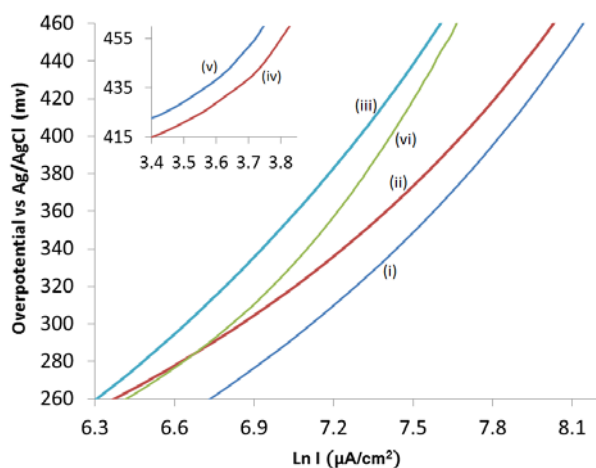


Figure 9. Tafel plots for: (i) PEDOT/nano-Ni/rGO containing 125 mg nano-Ni and 5.4 mg rGO (with light illumination), (ii) PEDOT/nano-Ni/rGO containing 125 mg nano-Ni and 5.4 mg rGO (without light illumination), (iii) control nano-Ni/rGO (without PEDOT) containing 125 mg nano-Ni and 5.4 mg rGO (with light illumination), (iv) control PEDOT only (with light illumination), (v) control PEDOT only (without light illumination), and (vi) control bare Pt.

Electrochemical Impedance Spectroscopy (EIS) and Tafel Plot studies of the PEDOT/Nano-Ni/rGO

To better understand the mechanism of the catalysis, we performed EIS and Tafel plot measurements on the most active PEDOT/nano-Ni/rGO electrode and compared them to the control films of nano-Ni/rGO (without PEDOT) containing 125 mg nano-Ni and 5.4 mg rGO, control bare Pt, and control PEDOT alone, with and without light illumination. The individual data points in Figure 8(a) and Figure 8(c) depict the measured data from the EIS studies. The bare Pt control produced haphazard, irreproducible data due, most likely, to interference arising from gas bubble formation, and is not depicted. Figure 9 shows the Tafel plots.

As can be seen in the Nyquist and corresponding Bode plots (Figures 8(a),(c)), the performance of the control PEDOT samples, with and without illumination, were governed by diffusion processes with frequencies about the $10^{0.5}$ Hz range. The nano-Ni/rGO and PEDOT/nano-Ni/rGO samples (with and without illumination) were, however, dominated by processes at intermediate frequencies ($10^{1-1.5}$ Hz), which are more typical of interfacial and solution catalytic charge transfer processes, like adsorption.⁵⁷ High frequency components at 10^{3-4} Hz were not observed (Figure 8(a) inset). It can be concluded that catalytic hydrogen generation by nano-Ni/rGO and PEDOT/nano-Ni/rGO (with and without light illumination) was kinetically controlled and involved the same catalytic sites.

Accordingly, we modelled the EIS data using the equivalent circuit depicted in Figure 8(b), as used previously.⁵⁷⁻⁶³ The modelled data is shown as the solid lines in Figure 8(a). As can be seen, there is an excellent match between the measured data and the modelled data. Table 1 provides results deriving from the modelling, including the ohmic resistance, R_o , solution/interfacial/charge transfer resistance, R_{ct} , and capacitance, which was expressed in terms

Sample	R_o (Ω cm^2)	R_{ct} (Ω cm^2)	Q_{CPE} ($\mu\Omega^{-1}cm^{-2}s^n$)	n_{CPE}	C_{CPE} (μFcm^{-2} $\times 10^4$)	A (mV/dec)	i_o (μA cm^2)
PEDOT (dark)	43.57	1005	96.32	0.80	2.43	70.24	14.80
PEDOT (light)	42.81	749.2	105.0	0.80	2.69	68.31	15.74
Nano-Ni/rGO (light)	45.84	265.6	142.0	0.81	4.20	58.72	9.07
PEDOT/nano-Ni/rGO (dark)	43.38	189.5	156.0	0.80	4.25	57.74	6.45
PEDOT/nano-Ni/rGO (light)	42.43	173.8	165.0	0.81	4.71	47.83	6.67
Pt	----	-----	-----	----	-----	58.35	7.02

Table 1. Data from modelling of the EIS results in Figure 8 (ohmic resistance, R_o , charge transfer resistance, R_{ct} , and charge transfer capacitance (C_{ct}) expressed in terms of a constant phase element (n_{CPE} , and C_{CPE}),⁶⁴ and Tafel plots (slope A; exchange current density i_o). The equivalent circuit in Figure 8(b) was used to model the EIS data. ('dark' = without light illumination; 'light' = with light illumination).

of a constant phase element (n_{CPE} , and C_{CPE}).⁶⁴ The constant phase element provided the best fit of the measured and modelled data.

The value of C_{CPE} shows a notable increase in going from control PEDOT to the nano-Ni/rGO film, to the PEDOT/nano-Ni/rGO film, without and, then, with light illumination. This indicates that the PEDOT/nano-Ni/rGO film had a slightly greater active area than the nano-Ni/rGO film, and a much greater active area than the control PEDOT alone. Illumination of the PEDOT/nano-Ni/rGO with light still further increased its active area.

The PEDOT/nano-Ni/rGO also exhibited more efficient catalysis at -0.75 V vs Ag/AgCl, as demonstrated by a lower R_{ct} ($173.8 \Omega cm^2$ with light illumination; vs $189.5 \Omega cm^2$ without light illumination and $265.6 \Omega cm^2$ for the nano-Ni/rGO film). The control PEDOT was substantially less active as evidenced by very high R_{ct} values ($1005 \Omega cm^2$ with light illumination, and $749.2 \Omega cm^2$ without light illumination). The ohmic resistance R_o was similar for each sample, falling in the range $42.43-45.84 \Omega cm^2$.

Figure 9 depicts Tafel plots for the catalysts, with results tabulated in the last two columns of Table 1.

The exchange current density, i_o , indicates the (intrinsic) catalytic rate of each material at the reversible potential, with an overpotential of zero. As can be seen, the control PEDOT exhibited the highest i_o indicating it to be a good HER catalyst ($14.80 \mu A/cm^2$ without light illumination; $15.74 \mu A/cm^2$ with light illumination). The nano-Ni/rGO (without PEDOT) exhibited the highest i_o of the metal-containing catalysts ($9.07 \mu A/cm^2$), with the bare Pt control following behind ($7.02 \mu A/cm^2$). The PEDOT/nano-Ni/rGO samples with and without light illumination were, in fact, the least intrinsically active. However, their lower Tafel slopes (A), particularly that of PEDOT/nano-Ni/rGO under light illumination, meant that their catalytic activity was more strongly accelerated by the applied bias than the control nano-Ni/rGO and control Pt samples.

The catalytic activity at -0.75 V (vs Ag/AgCl) was $3.6 mA/cm^2$ for PEDOT/nano-Ni/rGO vs. $2.1 mA/cm^2$ for the same quantities of nano-Ni/rGO without the PEDOT. That is, the presence of the PEDOT increased the catalytic rate by $1.5 mA/cm^2$, which equates to

a 71% increase. The PEDOT/nano-Ni/rGO was also 64% more active than a benchmark, control bare Pt electrode under identical conditions, which produced 2.2 mA/cm². The above thin-film appears to be the most active PEDOT-based HER catalyst yet reported as a proportion of the catalytic activity of Pt under the same conditions.

Accordingly, it can be concluded that the catalytic amplification exhibited by the PEDOT/nano-Ni/rGO film relative to the PEDOT-free nano-Ni/rGO control derived from a larger active area that was, additionally, strongly activated by the voltage bias (yielding a lower Tafel slope).

The Mechanism and Origin of the Catalytic Amplification

At -0.75 V, PEDOT is in its non-conducting form, meaning that it does not formally have a capacity to conduct electrons. However, in this state, PEDOT is an excellent hole (h⁺) transport material, meaning that holes formed on the PEDOT backbone can migrate to the FTO surface.

The catalytic mechanism therefore likely involved protons (H⁺) being converted to hydrogen (H₂) on catalytic sites in the thin film coating, with electrons being extracted from a nearby PEDOT monomer to facilitate this process. The resulting holes (h⁺) then migrated along the PEDOT chain to the surface of the FTO slide, where they were quenched by electrons provided via the external circuit. The rate at which holes formed and migrated through the PEDOT to the external circuit would, undoubtedly, have been strongly affected by the applied bias. Instead of the PEDOT acting as an electron conductor, it therefore appears to have acted as a semi-conductor, providing electrons and transporting the resulting holes to the external circuit.

While the mechanism of charge transport by the PEDOT did not involve electron conduction, it is, nevertheless, clear that the catalytic amplification exhibited by the PEDOT/nano-Ni/rGO film relative to the nano-Ni/rGO control (without PEDOT), derived from a larger active area that was, additionally, more strongly activated by the voltage bias (yielding a lower Tafel slope). That is, in connecting the maximum number of catalytically active sites to the external circuit, the PEDOT maximally increased the electrochemically active area of the catalyst. In providing a pathway for charge carrier exchange from each of those catalytic sites to the external circuit, the PEDOT also made each catalytic site more responsive to the applied bias (i.e. it better transmitted the bias). It did this by acting like a semiconductor.

The question that then arises is: why was there the extreme sensitivity to the precise quantity of rGO present? That is, why did the inclusion of 5.4 mg rGO yield a notably higher current density than 6.0 mg or 4.8 mg? Comparisons of the EIS data of the above films were inconclusive in respect of explaining their different catalytic performances.

A possible clue in this respect may be found in a comparison of the thicknesses and (electron) conductivities of the different films. As shown in Table 2, the coating with 5.4 mg rGO was notably thinner than the coating with 6.0 mg rGO. However, the (electron) conductivity and therefore, likely, also the hole transport

Film	Thick-ness μm	Conduct-ivity S/cm ²
PEDOT/nano-Ni/rGO (4.8 mg)	0.61-0.63	8.30
PEDOT/nano-Ni/rGO (5.4 mg)	0.61-0.63	8.53
PEDOT/nano-Ni/rGO (6.0 mg)	0.63-0.65	8.56
Nano-Ni/rGO (5.4 mg)	0.58-0.59	3.80

Table 2. Measured conductivity and thickness of the PEDOT thin films containing 125 mg nano-Ni and 4.8 mg, 5.4 mg, or 6.0 mg rGO.

properties, of the two coatings were very similar (both being broadly controlled by the linearity of the PEDOT chains). By contrast, the coating with 4.8 mg rGO was also thin, but its conductivity, and therefore, likely, also its hole transport capability was notably lower. This data therefore suggests that the coating with 5.4 mg rGO combined the thinnest layer with the highest hole transport conductivity. That is, it appears that this coating combined the highest density of catalytic sites with the shortest pathway for charge carrier movement to the external circuit. While the coatings swell and become thicker during operation, as noted earlier, this seems to involve the PEDOT itself opening up to form vacant, nanoscopic pores, so that the structure of the body of the coating does not seem to change significantly.

The synergistic effect therefore appears to have derived from a very particular ratio of catalyst density to film conductivity and thickness. In this respect, the above results conform with the concept¹¹ that a thin-film conducting polymer may potentially be induced to amplify catalytic performance by optimizing the ratio of catalyst density to film conductivity and thickness.

Conclusions

Thin, vapour phase polymerized PEDOT films containing nano-Ni and rGO, on FTO glass, were examined as (photo)electrocatalysts of hydrogen generation. Composite thin-films incorporating PEDOT : nano-Ni : rGO having 5.6 (C; PEDOT) : 1 (Ni) : 5.2 (C; rGO) molar ratios yielded current densities of 3.6 mA/cm² (including ca. 200 μA/cm² due to light illumination) after 3 h at -0.75 V (vs Ag/AgCl) under 0.25 sun in 0.05 M H₂SO₄/0.2 M Na₂SO₄. The PEDOT substrate of the above film made a substantial contribution to this catalytic performance as demonstrated by the fact that, under identical conditions after 3 h, a nano-Ni/rGO film of equivalent composition, that did not contain PEDOT, generated only 2.1 mA/cm². Moreover, a comparable Pt thin film yielded only 2.2 mA/cm² after 3 h under identical conditions. Equivalent control PEDOT, PEDOT/nano-Ni, and PEDOT/rGO films were an order of magnitude less catalytically active. Studies indicated that the PEDOT brought about the amplification by connecting the largest number of catalytic sites (nano-Ni) by the shortest possible pathways to the external circuit. The rGO may also have acted as catalytic sites. Gas chromatography confirmed that hydrogen was the sole gas produced by the most active PEDOT/nano-Ni/rGO thin film. SEM/EDX indicated that the above film displayed a structure, in which the PEDOT largely bridged and bound the component materials present. TEM indicated that the PEDOT formed an apparently seamless

interface with the nano-Ni lattice and rGO platelets. XRD and XPS analyses confirmed the elemental composition and chemical structure of the composite. In demonstrating that a particular ratio of catalyst density to film conductivity and thickness was needed for the observed catalytic amplification, this work was consistent with earlier propositions to the same effect.¹¹ The extreme sensitivity of the catalytic amplification to the precise composition of the thin film attests to the synergistic nature of the effect.

Experimental

Materials and Techniques

The following materials were used (Supplier): Fluorine-doped tin oxide (FTO) slides (Zhuhai Kaivo Electronic Components Co.); glass microscope slides (Australia Optics); iron(III) *p*-toluenesulfonate (Fe(III)-pTS) (technical grade, Sigma Aldrich Co.); 3,4-ethylenedioxythiophene (EDOT) (97%, Sigma Aldrich Co.); graphite flakes (3772) (Asbury Graphite Mills USA), Ni nanoparticles (99.9%, 20 nm; Skyspring Nanomaterials, Houston).

FTO and glass substrates were cleaned using a PLAMAFLO PDC-FMG Plasma cleaner and a DIG UV PSD PR SERIES digital UV Ozone cleaner. Sonication was carried out using a B2500R-MTH sonicator. Spin-coating onto the substrates was carried out using a WS-400B-6NPP/LITE spin-coater. Centrifugation-washing steps were carried out using a ProSciTech TG16WS centrifuge.

Thickness measurements were made using a Vccco Dektak 150 profilometer. The electrical resistivity of the films after deposition, were measured on a non-conducting glass slide using an HG29315 Jandel equipped with a four-point probe. The resistivity (in Ω/\square) was calculated using the formula $\rho = t \cdot R_s$, where ρ is resistivity, t is sheet thickness and R_s is sheet resistance. Resistivity can then be converted to conductivity (S/cm). Scanning Electron Microscopy (SEM) and Transmission Electron Microscopy (TEM) images were taken using a JEOL 7500 FESEM. Elemental analysis was done by the Campbell Microanalytical laboratory at the University of Otago, New Zealand. Powder X-ray diffraction (XRD) patterns of GO, rGO, PEDOT and PEDOT/nano-Ni/rGO were recorded on a GBC MMA instrument using Cu K α radiation with $\lambda = 1.5418 \text{ \AA}$ at scan rate of 2% min over the range 8-80°. X-ray photoelectron spectroscopy was carried out on a PHI660 instrument using a monochromatic Mg K α X-ray source.

GO synthesis

In order to prepare fully oxidized graphite, dry expandable graphite flakes were first thermally treated at 700 °C in a vertical tube furnace under N₂ atmosphere. The resulting expanded graphite (EG) was used as a precursor for GO synthesis, following previously described methods.⁶⁵⁻⁶⁹ Briefly, 1 g of EG and 200 mL of H₂SO₄ were mixed and stirred in a flask for 24 h. KMnO₄ (5 g) was then added to the mixture slowly. The mixture was transferred into an ice bath and 200 mL of DI water containing 50 mL of 30% H₂O₂ were poured slowly into the mixture. The suspension changed colour to light brown. After stirring for another 30 min, the resulting GO particles were washed and centrifuged with a HCl solution (9:1 water: c.HCl by volume), then centrifuged again and washed with DI water until

the pH of the solution became 3 - 4. The resultant GO sheets were dispersed in deionized water by gentle shaking. Then, a GO dispersion in ethanol was prepared by extracting the water from the parent aqueous GO dispersion by repeated centrifugation-washing steps (6 times, for 10 - 30 min each, at 11000 rpm).⁷⁰ The parent aqueous GO (15 mL) ($\sim 2.5 \text{ mg ml}^{-1}$) was poured into a 50 ml centrifuge tube (Nalgene), to which 20 ml ethanol was added, followed by vigorous mixing using a vortex shaker. After each centrifuging, 30 ml of the supernatant was poured off and replaced with 30 ml of ethanol and then mixed vigorously by vortex shaking. This process was repeated a further 5 times to replace the water with ethanol. Finally, the dispersion was sonicated in a bath sonicator for 1 h before being centrifuged again to make a high concentration dispersion ($\sim 30 \text{ mg/ml GO}$).

Preparation of PEDOT, PEDOT/nano-Ni, PEDOT/rGO, PEDOT/nano-Ni/rGO and Nano-Ni/rGO on FTO-coated glass slides

Uncoated glass and FTO-coated glass slides were immersed in acetone within a TLC chamber. The baths with the immersed slides were sonicated for 90 min, whereafter the slides were washed with water and dried by blowing air over them. The FTO and uncoated glass slides were then labelled. All slides were thereafter treated in a digital ozone-UV cleaner for 20 min to remove organic contaminants. The slides were then cleaned in a plasma cleaner in order to functionalize groups on the slide's surface with which to fix the coated chemical solutions during spin-coating. The FTO and glass substrates were heated to dryness on an IKA® RCT basic hotplate at 60 °C.

To prepare the PEDOT, PEDOT/nano-Ni, PEDOT/rGO, and PEDOT/nano-Ni/rGO films on FTO glass slides, the following procedure was used. Where applicable, GO ethanol solution (e.g. 0.2 ml) was transferred to a small glass vial and the volume increased to 1.2 ml by adding absolute ethanol. The solution was sonicated for 10 min and then stirred with a magnetic stirrer for 5 min. Where applicable, Nano-Ni (e.g. 125 mg) was added gradually with magnetic stirring continuing for 2.5 h thereafter. A solution of dissolved Fe(III)-PTS (100 mg) in 0.15 ml ethanol was then added to the mixture. The resulting solution (100 μL) was dropcast onto the slide surface using a micropipette. The slides were then spun at 2000 revolutions per minute (rpm) for 180 s. After spin-coating, the sample was quickly transferred to a hotplate, where it was dried at 60 °C for 15 min.

Vapour phase polymerisation was carried out in a separate conical flask (500 mL capacity), equipped with a rubber stopper containing a crocodile clip suspended above the bottom of the flask. EDOT (0.450 mL) was placed in the flask and the dried, spin-coated FTO or uncoated glass substrates were held above the EDOT solution by the crocodile clip, with the stopper in place. The stoppered conical flask was then placed in an oven at 60 °C for 60 min, during which time the EDOT vapour polymerised into PEDOT polymer on the slide surface. After polymerisation was complete, the sample was removed, washed thoroughly with ethanol, and then left to dry overnight. A representative film of this type was 0.67 mm thick, with a conductance of 8.3 S/cm (on non-conducting glass).

The resulting dried FTO-coated samples were converted to usable electrodes by attaching a copper wire to the FTO surface with conductive silver paint and epoxy resin. When the silver paste was fully solidified, epoxy glue was used to cover the contact area of the wire as well as any exposed clean FTO glass surface.

Control nano-Ni/GO films on FTO were prepared by a similar process, without adding Fe(III)-PTS to the spin-coating solution or exposing the spin-coated layer to EDOT vapour. The spin-coated nano-Ni/GO films proved to be robustly attached to the FTO glass and durable to subsequent electrochemical testing.

Immediately prior to testing as a (photo)electrocatalyst, the GO present in all films was reduced electrochemically to rGO using cyclic voltammetry (performed in 0.2 M Na₂SO₄ (pH 12); 5 cycles between -1.2 to 0.8 V, vs. Ag/AgCl, at 50 mV/s scan speed) (Figure S5, Figure S6).

Studies of PEDOT/Nano-Ni, PEDOT/Nano-Ni/rGO and Nano-Ni/rGO on FTO as HER Photocatalysis

The resulting nanocomposite mixtures on the FTO-coated glass slides were employed as working electrodes within a fully-enclosed quartz cell (5 x 5 x 5 cm) placed inside a closed cabinet that comprised a Faraday cage. A Pt mesh (1 x 2 cm) was used as the counter electrode. A BASi Ag/AgCl aqueous salt bridge (KCl, 3 M) served as reference electrode. The electrolyte employed was a 0.2 M Na₂SO₄/0.05 M H₂SO₄ aqueous solution, adjusted to pH1 by adding H₂SO₄. The electrolyte was bubbled with N₂ gas for 30 min before each experiment. Linear sweep voltammetry (LSV), cyclic voltammetry (CV) and chronoamperograms (CA) were performed using an EDAQ466 potentiostat. Where applicable, the sample was illuminated with a SoLux daylight MR16 halogen light bulb (12 V, 50 W, 24°; 0.25 sun intensity) with a stable output range of 275 - 750 nm. The light was placed 10 cm from the working electrode. A Thorlabs visible-light bandpass filter (315-710 nm) was placed 1.5 cm in front of the light source. The bandpass filter removed any heat (infra-red wavelengths) generated by the light source.

Electrochemical Impedance studies (EIS) were conducted potentiostatically at -0.75 V (vs. Ag/AgCl) under the same conditions as the amperometric studies, with the same light source, applying frequencies between 0.1 Hz and 150 KHz.

Gas Analysis Studies

Photocurrent testing of high performing PEDOT/Nano-Ni/rGO samples on FTO glass with simultaneous gas analysis was performed using a custom-built apparatus. The apparatus, which is depicted in Figure S1, comprised of a fully-enclosed electrochemical cell containing two sealed, gas-tight half-cells whose electrolytes were separated only by a Nafion 117 proton exchange membrane (5 x 4 cm). The one half cell contained the working electrode sample and a Ag/AgCl reference electrode. The other half-cell contained the Pt mesh counter electrode. One wall of the former half-cell was a quartz sheet. Illumination from the above light source was passed through the quartz sheet onto the working electrode. The incident light was filtered with the above bandpass filter. The electrodes were connected to a CHI potentiostat. The gas outlets for the working and counter electrode were connected with stainless steel

tubing to sample loops connected to a dedicated Shimadzu GC-8A gas chromatograph.

After fitting the electrodes, both half cells were filled with electrolyte. The electrolyte in each half cell was then separately purged with Ar gas overnight to remove all air inside the cell (without a voltage or light-illumination being applied to the cell). Thereafter, the Ar passing through each half cell was sampled, injected and analysed using the attached gas chromatograph, with the results plotted over 30 min of elution time. The analyses verified that there was no gas other than Ar in the gas streams passing through each half-cell. The Ar gas, which was continuously bubbled through the electrolyte throughout the photocurrent experiment, acted as a carrier gas for the connected GC.

Voltage and light-illumination was then applied to the cell, whereafter the carrier gas was tested as described above, for electrocatalysis product gases using the GC. The identities of the gases in the carrier Ar were determined by their retention times. GC testing of this type, after illumination and biasing, provided a quantitative measure of the gases produced by photoelectrochemical activity of the samples.

Conflicts of interest

There are no conflicts to declare.

Acknowledgements

MA thanks the Government of Iraq for a PhD scholarship. The authors thank A/Prof Attila Mozer of the University of Wollongong for use of a GC gas analyser. The authors acknowledge the Australian National Fabrication Facility (ANFF) Materials Node for equipment use and Mr Adam Taylor for design and printing of the custom-built apparatus. Support from the Australian Research Council Centre of Excellence Scheme (Project Number CE140100012) is gratefully acknowledged. The authors acknowledge use of facilities and the assistance of Tony Romeo within the University of Wollongong Electron Microscopy Centre. This research used equipment funded by the Australian Research Council (ARC) – Linkage, Infrastructure, Equipment and Facilities (LIEF) grant LE160100063 located at the University of Wollongong Electron Microscopy Centre.

Notes and references

- 1 A. Züttel, A. Remhof, A. Borgschulte, O. Friedrichs, *Phil. Trans. R. Soc. A.*, 2010, **368**, 3329.
- 2 J. M. Ogden, *Phys. Today* 2002, **55**, 69.
- 3 C. S. W. Jeffrey, H. Chao-Wei, L. Chi-Hung *Catal.* 2012, **2**, 490.
- 4 G. Grace, *Petroleum Rev.* 2004, **57**, 32.
- 5 (a) M. Alsultan, A. Ranjbar, G. F. Swiegers, G. G. Wallace, S. Balakrishnan, J. Huang, Chap 11 in *Industrial Applications for Intelligent Polymers and Coatings*, M. Hosseini, A. S. H. Makhlof (eds.), Springer International Publishing, Switzerland, 2016, and refs therein; (b) B. Winther-Jensen, D. R. MacFarlane, *Energy Environ. Sci.*, 2011, **4**, 2790.
- 6 X. Long, Z. Wang, T. Zhang, S. Xiao, S. Yang, G. Li, H. Zhu, W. Guo, *J. Am. Chem. Soc.* 2015, **137**, 11900; O. Pyskhina, A.

- Kubarkov, V. Sergeyev, *Mat. Sci. Appl. Chem.* 2010, **21**, 51; A. Kros, N. A. J. M. Sommerdijk, R. M. Nolte, *Sens. Actuators* 2005, **106**, 289; C. Carlberg, X. Chen, O. Inganäs, *Solid State Ionics*, 1996, **85**, 73.
- 7 (a) C. Gu, B. Norris, F. Fan, C. Bielawski, A. Bard, *ACS Catalysis*, 2012, **2**, 746; (b) B. Winther-Jensen, K. Fraser, C. Ong, M. Forsyth, D. R. MacFarlane, *Adv. Mater.*, 2010, **22**, 1727.
- 8 K. Xie, H. Wu, Y. Meng, K. Lu, Z. Wei, Z. Zhang, *J. Mater. Chem.*, 2015, **3**, 78.
- 9 R. K. Pandey, V. Lakshminarayanan, *J. Phys. Chem. C*, 2010, **114**, 8507.
- 10 X. Li, W. Lu, W. Dong, Q. Chen, D. Wu, W. Zhou, L. Chen, *Nanoscale*, 2013, **5**, 5257.
- 11 M. Alsultan, S. Balakrishnan, J. Choi, R. Jalili, P. Tiwari, P. Wagner, G. F. Swiegers submitted for publication
- 12 G. Wang, B. Wang, J. Park, J. Yang, X. Shen, J. Yao, *Carbon* 2009, **47**, 68. K. Haubner, J. Murawski, P. Olk, L. Eng, C. Ziegler, B. Adolph, E. Jaehne, *ChemPhysChem*. 2010, **11**, 2131.
- 13 I. Khalil, N. M. Julkapli, W. A. Yehye, W. J. Basirun, S. K. Bhargava, *Materials* 2016, **9**, 406.
- 14 D. Sharma, S. Kanchi, M. I. Sabela, K. Bisetty, *Arab. J. Chem.*, 2016, **9**, 238.
- 15 B. Devadas, M. Rajkumar, S.-M. Chen, R. Saraswathi, *Int. J. Electrochem. Sci.*, 2012, **7**, 3339.
- 16 K. H. Kim, M. Yang, K. M. Cho, Y. S. Jun, S. B. Lee, H. T. Jung, *Sci. Rep.* 2013, **3**, 3251.
- 17 A number of HER catalysts incorporating rGO have been reported; see for example: (a) G. Xie, K. Zhang, B. Guo, Q. Liu, L. Fang, J. R. Gong, *Adv. Mater.* 2013, **25**, 3820, and ref. therein; (b) X. Zou, Y. Zhang, *Chem. Soc. Rev.* 2015, **44**, 5148 and ref. therein. Space precludes a full listing of HER catalysts incorporating rGO; representative examples are provided in ref. 18-24.
- 18 Y. Li, H. Wang, L. Xie, Y. Liang, G. Hong, H. Dai, *J. Am. Chem. Soc.* 2011, **133**, 7296
- 19 F. Meng, J. Li, S. K. Cushing, M. Zhi, N. Wu, *J. Am. Chem. Soc.* 2013, **135**, 10286; H. Tang, K. Dou, C.-C. Kaun, Q. Kuanga, S. Yang, *J. Mater. Chem. A*, 2014, **2**, 360; X. Zheng, J. Xu, K. Yan, H. Wang, Z. Wang, S. Yang, *Chem. Mater.* 2014, **26**, 2344; C.-B. Ma, X. Qi, B. Chen, S. Bao, Z. Yin, X.-J. Wu, Z. Luo, J. Wei, H.-L. Zhang, H. Zhang, *Nanoscale*, 2014, **6**, 5624; S. Peng, L. Li, X. Han, W. Sun, M. Srinivasan, S. G. Mhaisalkar, F. Cheng, Q. Yan, J. Chen, S. Ramakrishna, *Angew. Chem. Int. Ed.* 2014, **53**, 12594; Y.-J. Tang, M.-R. Gao, C.-H. Liu, S.-L. Li, H.-L. Jiang, Y.-Q. Lan, M. Han, S.-H. Yu, *Angew. Chem. Int. Ed.* 2015, **54**, 12928; Y. Li, H. Wang, S. Peng, *J. Phys. Chem. C* 2014, **118**, 19842.
- 20 H. Yan, C. Tian, L. Wang, A. Wu, M. Meng, L. Zhao, H. Fu, *Angew. Chem. Int. Ed.* 2015, **54**, 6325
- 21 L. Jiao, Y.-X. Zhou, H.-L. Jiang, *Chem. Sci.*, 2016, **7**, 1690; L. Ma, X. Shen, H. Zhou, G. Zhu, Z. Jia, K. Chen, *J. Mater. Chem. A*, 2015, **3**, 5337; Y. Pan, N. Yang, Y. Chen, Y. Lin, Y. Li, Y. Liu, C. Liu, *J. Power Sources*, 2015, **297**, 45
- 22 S. Chandrasekaran, W. Choi, J. Chung, S. Hur, E. Kim, *Mater. Lett.* 2014, **136**, 118; Y. Li, H. Wang, S. Peng, *J. Phys. Chem C*. 2014, **118**, 19842
- 23 X. Liu, W. Liu, M. Ko, M. Park, M. G. Kim, P. Oh, S. Chae, S. Park, A. Casimir, G. Wu, J. Cho, *Adv. Funct. Mater.* 2015, **25**, 5799; J. Zhang, Q. Wang, L. Wang, X. Li, W. Huang, *Nanoscale*, 2015, **7**, 10391; D. Chanda, J. Hnat, A. Dobrota, I. Pasti, M. Paidar, K. Bouzek, *Phys. Chem. Chem. Phys.*, 2015, **17**, 26864.
- 24 R. Chen, Y. Song, Z. Wang, Y. Gao, Y. Sheng, Z. Shu, J. Zhang, X. Li, *Cat. Commun.*, 2016, **85**, 26; B. Rezaei, A. Jahromi, A. Ensafi, *Electrochimica Acta.*, 2016, **213**, 423. Y. Tang, Y. Wang, X. Wang, S. Li, W. Huang, L. Dong, C. Liu, Y. Li, Y. Lan, *Adv. Energy Mater.*, 2016, **6**, 1; D. Chen, L. Zou, S. Li, F. Zheng, *Sci. Rep.*, 2016, **6**, 20335;
- 25 J. Chen, P. W. Wagner, L. Tong, D. Boskovic, W. Zhang, D. L. Officer, G. G. Wallace, G. F. Swiegers, *Chem. Sci.*, 2013, **4**, 2797.
- 26 See, for example: J. Chen, J. Huang, G. F. Swiegers, C. O. Too, G. G. Wallace, *Chem. Commun.* 2004, 308.
- 27 Z.-A. Hu, Y.-L. Xie, Y.-X. Wang, H.-Y. Wu, Y.-Y. Yang, Z.-Y. Zhang, *Electrochim. Acta*, 2009, **54**, 2737.
- 28 X. Liu, J. Huang, X. Wei, C. Yuan, T. Liu, D. Cao, J. Yin, G. Wang, *J. Power Sources*, 2013, **240**, 338.
- 29 Y. Zhao, S. He, M. Wei, D. G. Evans, X. Duan, *Chem. Commun.*, 2010, **46**, 3031.
- 30 J. Xu, S. Gai, F. He, N. Niu, P. Gao, Y. Chen, P. Yang, *J. Mater. Chem. A*, 2014, **2**, 1022.
- 31 K. Satheesh, R. Jayavel, *Mater. Lett.* 2013, **113**, 5.
- 32 R. Gupta, Z. Alahmed, F. Yakuphanoglu, *Mater. Lett.*, 2013, **112**, 75.
- 33 T. Kavinkumar, S. Manivannan, *Ceramics International*, 2016, **42**, 1769.
- 34 K. Muthoosamy, R. Geetha Bai, S. Sudheer, S. Manickam, I. Abubakar, H. Loh, H. Lim, N. Huang, C. Chia, *Int. J. Nanomedicine*, 2015, **10**, 1505.
- 35 M. Zong, Y. Huang, Y. Zhao, X. Sun, C. Qu, D. Luo, J. Zheng, *RSC Adv.*, 2013, **45**, 23638.
- 36 Y. C. Si, E. T. Samulski, *Chem. Mater.*, 2008, **20**, 6792.
- 37 L. Zhang, R. Jamal, Q. Zhao, M. Wang, T. Abdiryim, *Nanoscale Res. Lett.* 2015, **10**, 148.
- 38 S. Jo, Y. Lee, J. Yang, W. Jung, J. Kim. *Synth. Met.*, 2012, **162**, 1279.
- 39 Z. Jiang, J. Xie, D. Jiang, X. Wei, M. Chen, *CrystEngComm*, 2013, **15**, 560.
- 40 Z. Wei, J. Ma, W. Feng, J. Dai, Q. Wang, T. Xia, P. Yan, *Mater. Characterization*, 2007, **58**, 1019.
- 41 K. Dave, K. H. Park, M. Dhayal, *RSC Adv.*, 2015, **5**, 95657.
- 42 J. Lu, Y. Li, S. Li, S. Jiang, *Scientific Reports*, 2016, **6**, Article Number: 21530.
- 43 D. Mhamane, M. Kim, H. Kim, D. Ruan, K. Kim, V. Aravindan, M. Srinivasan, K. Roh, S. Lee, *J. Mater. Chem. A*, 2016, **4**, 15, 5578.
- 44 K. Yuan, M. Forster, U. Scherf, Y. Xu, M. Que, Y. Chen, J. Uihlein, T. Chassé, G. Brunklaus, L. Shi, T. Pichler, R. Heiderhoff, T. Riedl, *Adv. Mater.*, 2015, **27**, 6714.
- 45 A. Shaikh, S. Parida, S. Böhm, *RSC Adv.*, 2016, **6**, 100383.
- 46 P. Benjwal, P. Chamoli, K. Kar, M. Kumar, *RSC Adv.*, 2015, **5**, 73249.
- 47 L. Wang, Y. Li, Z. Han, B. Qian, X. Jiang, G. Yang, L. Chen, J. Pinto, *J. Mater. Chem. A*, 2013, **1**, 8385.
- 48 J. E. Choe, M. S. Ahmed, S. Jeon, *J. Power Sources*, 2015, **281**, 211.
- 49 H. Park, S. J. Lee, S. Kim, H. W. Ryu, S. H. Lee, H. H. Choi, I. W. Cheong, J. Kim, *Polymer*, 2013, **54**, 4155.
- 50 M. Wang, M. Zhou, L. Zhu, Q., Li, C. Jiang, *Solar Energy*, 2016, **129**, 175.
- 51 T. Ji, L. Tan, X. Hu, Y. Dai, Y. Chen, *Phys. Chem. Chem. Phys.*, 2015, **17**, 4137.
- 52 A. Kanwat, J. Jang, *J. Mater. Chem. C*, 2014, **2**, 901.
- 53 A. Bagri, V. Shenoy, C. Mattevi, M. Chhowalla, M. Acik, Y. Chabal, *Nature Chem.*, 2010, **2**, 581.
- 54 V. Sridhar, I. Lee, H. Chun, H. Park, *RSC Adv.*, 2015, **5**, 68270.
- 55 Z. Xing, Z. Ju, Y. Zhao, J. Wan, Y. Zhu, Y. Qiang, Y. Qian, *Scientific Reports*, 2016, **6**, Article Number: 26146.
- 56 H. Yu, B. Zhang, C. Bulin, R. Li, R. Xing, 2016, *Scientific Reports*, 2016, **6**, Article Number: 36143.
- 57 A. A. Ensafi, E. Heydari-Soureshjani, M. Jafari-Asl, B. Rezaei, *Carbon* 2016, **99**, 398.
- 58 H. Nady, M. Negema *RSC Adv.*, 2016, **6**, 51111.

- 59 Y. Qiang, L. Guo, S. Zhang, W. Li, S. Yu, J. Tan, *Scientific Reports*, 2016, **6**, article number: 33305.
- 60 F. Fiegenbaum, M. O. de Souza, M. R. Becker, E. M. A. Martini, R. F. de Souza, *J. Power Sources*, 2015, **280**, 12.
- 61 H. Jafari, K. Akbarzade, I. Danaee, *Arabian J. Chem.* 2014; DOI: 10.1016/j.arabjc.2014.11.018.
- 62 B. Ren, D. Li, Q. Jin, H. Cui, C. Wang, *J. Mater. Chem. A*, 2017, **5**, 13196.
- 63 B. Konkana, K. Junge Puring, I. Sinev, S. Piontek, O. Khavryuchenko, J. P. Dürholt, R. Schmid, H. Tüysüz, M. Muhler, W. Schuhmann, U.-P. Apfel, *Nature Comm.* 2016, **7**, 12269.
- 64 G. J. Brug, A. L. G. van den Eeden, M. Sluyters-Rehbach, J. H. Sluyters, *J. Electroanal. Chem.* 1984, **176**, 275.
- 65 D. Esrafilzadeh, R. Jalili, E. Stewart, J. Razal, S. Moulton, G. G. Wallace, S. Aboutalebi, *Adv. Funct. Mat.*, 2016, **26**, 3105.
- 66 R. Jalili, D. Esrafilzadeh, R. Shepherd, J. Chen, J. Razal, G. G. Wallace, S. Aboutalebi, S. Aminorroaya-Yamini, K. Konstantinov, A. Minett, *Adv. Funct. Mat.*, 2013, **23**, 5345.
- 67 R. Jalili, S. H. Aboutalebi, D. Esrafilzadeh, K. Konstantinov, J. M. Razal, S. E. Moulton, G. G. Wallace, *Mater. Horiz.* 2014, **1**, 87.
- 68 S. Naficy, R. Jalili, S. Aboutalebi, R. Gorkin, K. Konstantinov, P. Innis, G. Spinks, P. Poulin, G. G. Wallace, *Mater. Horizon*, 2014, **1**, 326.
- 69 S. Gambhir, R. Jalili, D. L. Officer, G. G. Wallace, *NPG Asia Mater.*, 2015, **7**, e-186-1.
- 70 R. Jalili, D. Esrafilzadeh, S. Moulton, J. Razal, G. G. Wallace, S. Aboutalebi, K. Konstantinov, *ACS Nano*, 2013, **7**, 3981.